IET Communications

Research Article

IET Journals
The Institution of Engineering and Technology

Cooperative interference cancellation for cellular networks with imperfect CCSI

ISSN 1751-8628
Received on 15th September 2015
Revised on 15th November 2015
Accepted on 16th December 2015
doi: 10.1049/iet-com.2015.0897
www.ietdl.org

Refik Fatih Ustok[1] ✉, *Pawel A. Dmochowski*[1], *Peter J. Smith*[2], *Mansoor Shafi*[3]

[1]*School of Engineering, Victoria University of Wellington, Wellington 6012, New Zealand*
[2]*School of Mathematics, Statistics and Operations Research, Victoria University of Wellington, Wellington 6012, New Zealand*
[3]*Spark New Zealand, Wellington 6012, New Zealand*
✉ *E-mail: refik.ustok@ecs.vuw.ac.nz*

Abstract: In this study, the authors investigate the impact of cooperation in an interference limited downlink cellular network. The authors identify the areas in which the transmissions of adjacent cells overlap in a 19 cell network for urban and suburban environments. They assume that the cooperative users are located in these overlapping areas and thus can receive channel information from neighbouring base stations (BSs) to cancel intercell interference. They also study the performance of such systems with various types of precoding techniques. They demonstrate that they can improve the system performance employing precoders that maximise signal-to-leakage-noise ratios for each user. They also consider imperfect cross channel state information (CCSI) between cooperative users and interfering BSs. Furthermore, they analytically derive the additional intercell interference that is caused by imperfect CCSI at the receivers. The results demonstrate that the system can achieve better sum rates with cooperation, however this improvement is susceptible to the accuracy of the CCSI. They show that imperfect CCSI degrades the cooperation gains drastically.

1 Introduction

Next generation mobile wireless networks face increasing demand for higher data rates and a larger data volume. Therefore, there is an increasing need to build more efficient wireless networks, where many users share the same radio resources. Traditional interference management systems such as multiple access techniques do not allow us to use the radio resources efficiently [1]. Maham and Popovski [2] consider power control schemes for interference management with the assumption that intracell interference does not exist due to orthogonality of resource slots. Interference alignment (IA) has shown that each user can utilise the network resources more efficiently [1, 3]. However, IA requires an impractical number of signalling dimensions to achieve the optimal performance as the number of interferers increases [4]. Therefore, interference cancellation techniques should be used with IA techniques to relax the number of dimensions required.

IA and cancellation techniques have been studied in many types of uplink and downlink scenarios, including relay networks and cellular networks. In [5], an IA technique was proposed for a downlink cellular systems. The authors proposed a receiver which mimics minimum-mean-square-error (MMSE) and showed that it outperforms zero forcing (ZF) and matched filtering (MF) techniques in systems, where there are many interferers with different power levels. ZF precoders were used in [5] in order to align the intracell interference. In [6], the authors propose a combined receiver for uplink cellular networks. It is shown that the combined receiver outperforms the traditional MMSE receiver if the number of receive antennas is larger than the number of interfering streams. However, because of this antenna requirement, it is only practical for uplink systems.

Precoders have been used extensively to align and cancel interference. The idea of alignment is to design transmitted vectors so that they are aligned onto a linear subspace at the receiver [5]. ZF methods for MIMO interference channels are considered in [7]. ZF precoders require a condition on the number of transmit-receive antennas. According to this condition, the number of transmit antennas needs to be equal or larger than total number of receive antennas of the users to be nulled. If this condition is not satisfied, then the interference cannot be nulled. Signal to leakage-noise ratio (SLNR) based precoders are proposed in [8] in order to improve the system performance and relax the antenna number requirement.

Cell-edge spectral efficiency is very important in the design of cellular networks. In order to improve cell-edge spectral efficiency, the authors of [9–11] consider cooperation between the base stations (BSs). Currently coordinated multi-point transmission/reception systems allow coordination among three adjacent cells [12]. The coordination can be implemented in the overlapping regions where the coverage area of adjacent cells overlap. Guedes and Yacoub [13] show that the overlapping region can cover 30–47% of total area of two neighbouring cells. In [13], the overlapping region is assumed to be where the difference of the received power from two adjacent BSs is within 8 dB. We refer to the overlapping coverage area as the cooperation zone. In this paper, we consider cooperation between users in the cooperation zone and the neighbouring BSs. The users in the cooperation zone generate their postcoding vectors using cross channel state information (CCSI) to reduce the effect of the interference from the neighbouring cell BS. We refer this scheme as partial cooperative interference cancellation.

IA and cancellation techniques require perfect channel estimation [4]. It has been shown in [14, 15] that imperfect channel estimation causes misalignment of the interference. Therefore, we also consider the channel estimation error model given in [16] for interfering cross channels.

The contributions of this paper are:

- We propose a partial cooperative interference cancellation scheme based on the received powers from adjacent BSs. This enables us to assess the merits of varying mixtures of cooperative and non-cooperative users and the gains achievable while reducing the overhead of CCSI estimation between the interfering BS and the user.
- We demonstrate the mean sum rate gain that can be achieved by employing SLNR precoders compared with the ZF precoders of

© The Institution of Engineering and Technology 2016

[5] at low transmit SNR values where the noise is prominent. However, we also show that the mean sum rates of SLNR precoders approximate to those of ZF precoders at high transmit SNR values where the interference is prominent.

- To show the impact of environment type on the cooperation gains, we analyse our system for urban and suburban multicellular environments using the COST 231 Hata model. We demonstrate that the cooperation gains are different for different environments.
- We analytically derive expressions for the additional interference caused by imperfect CCSI and demonstrate its impact on the receiver performance in terms of mean sum rates, cooperation gains and outage probabilities.

This paper is organised as follows. The system model is described in Section 2. Section 3 presents the imperfect channel state information model and an analysis of its effects in the system. We discuss the different environments and we give simulation results in Section 4 and the conclusions are given in Section 5.

1.1 Notations

Throughout this paper, bold upper case and lower case letter denote a matrix and a vector, respectively, $(\cdot)^{\mathrm{T}}$ denotes transpose, $(\cdot)^*$ denotes the conjugate transpose and $\boldsymbol{I}$ denotes an identity matrix.

2 System model

We consider a 19 cell system with K randomly located users in each cell. Each user is equipped with N_{r} antennas while each BS is equipped with N_{t} antennas. The users experience both intracell and intercell interference. Precoding vectors, $\boldsymbol{v}$, are used to align intracell interference caused by transmissions to other users in the same cell, while postcoding vectors, $\boldsymbol{u}$, mitigate intercell interference caused by the neighbouring cells. The received signal of user i in cell α is given by

$$\boldsymbol{y}_{\alpha,i} = \left(\sqrt{\frac{\rho_{\alpha,i}}{K}}\right)\boldsymbol{H}_{\alpha,i}\bar{\boldsymbol{P}}\sum_{k=1}^{K}\boldsymbol{v}_{\alpha,k}x_{\alpha,k} + \sum_{\beta}\left(\sqrt{\frac{\rho_{\beta,i}}{K}}\right)\boldsymbol{G}_{\beta,i}\bar{\boldsymbol{P}}\sum_{l=1}^{K}\boldsymbol{v}_{\beta,l}x_{\beta,l} + \boldsymbol{z}_{\alpha,i} + \boldsymbol{n}_{\alpha,i}, \quad (1)$$

where the noise, $\boldsymbol{n}_{\alpha,i}$, is assumed to be $\mathcal{CN}(0, \boldsymbol{I})$. We define $\rho_{\alpha,i} = \upsilon\xi_{\alpha,i}$, where υ is the total transmit power of the BS and $\xi_{\alpha,i}$ is the attenuation due to path-loss and shadowing between the BS α and the user i. Because the noise has unit variance, υ can also be interpreted as the transmit SNR as in [5] [Note that SNR is usually defined at the receiver. However, in this case υ can be considered as logically equivalent to a transmit SNR as the noise variance is unity. This concept is also adopted in [5] and in a number of other papers.]. The dominant interference forms the second term in (1) which involves the summation over all dominant BSs indexed by β. $\boldsymbol{z}_{\alpha,i}$ denotes the remaining interference from all other, non-dominant cells. Each BS transmits its data using K precoding vectors, for example at BS α, $\boldsymbol{B}_{\alpha} = [\boldsymbol{v}_{\alpha,1}, \boldsymbol{v}_{\alpha,2}, \ldots, \boldsymbol{v}_{\alpha,K}] \in \mathbb{C}^{N_{\mathrm{t}}\times K}$, and a secondary precoding matrix $\bar{\boldsymbol{P}}$ is also used as in [5]. Using these two precoders, $\bar{\boldsymbol{P}}$ and $\boldsymbol{B}_{\alpha}$, BS α sends the complex symbols $(x_{\alpha,1}, x_{\alpha,2}, \ldots, x_{\alpha,K})$, intended for the users in cell α. $\boldsymbol{H}_{\alpha,i} \in \mathcal{CN}^{N_{\mathrm{r}}\times N_{\mathrm{t}}}(0, \boldsymbol{I})$ indicates the direct channel from BS α to user i of cell α and $\boldsymbol{G}_{\beta,i} \in \mathcal{CN}^{N_{\mathrm{r}}\times N_{\mathrm{t}}}(0, \boldsymbol{I})$ denotes the cross channel from an interfering BS, indexed by β.

The N_{t} by N_{t} secondary precoding matrix $\bar{\boldsymbol{P}}$ is used at the transmitters to colour the interference space [5]. This fixed precoder matrix is independent of the channel gains and is given by

$$\bar{\boldsymbol{P}} = \left[\boldsymbol{f}_1, \ldots, \boldsymbol{f}_S, \kappa\boldsymbol{f}_{S+1}, \ldots, \kappa\boldsymbol{f}_{N_{\mathrm{t}}}\right] \in \mathbb{C}^{N_{\mathrm{t}}\times N_{\mathrm{t}}}, \quad (2)$$

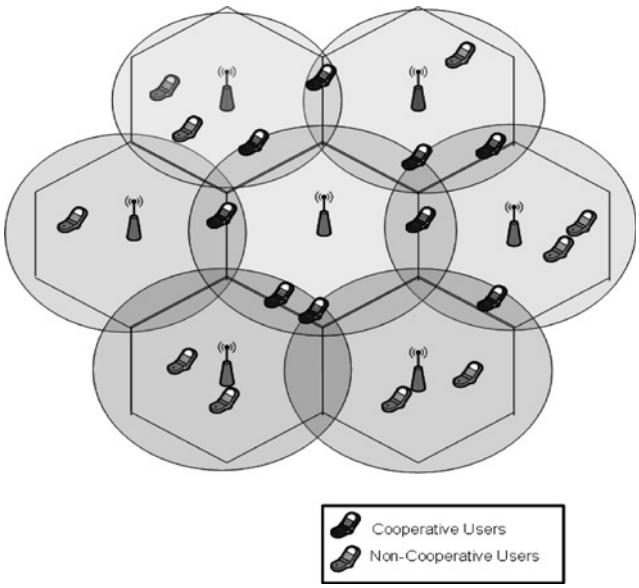

Fig. 1 *System model for cooperation*

where $[\boldsymbol{f}_1, \ldots, \boldsymbol{f}_{N_{\mathrm{t}}}]$ is a unitary matrix. In [5], κ is found heuristically based on simulation results using

$$\kappa = \min\left(\gamma^{1/4}, 1\right), \quad (3)$$

where the system parameter $\gamma = (\mathrm{INR}_{\mathrm{rem}}/\mathrm{INR}_{\mathrm{dom}})$ with $\mathrm{INR}_{\mathrm{dom}}$ and $\mathrm{INR}_{\mathrm{rem}}$ are the long term interference-to-noise ratios of the total dominant and remaining interference, respectively. In a multicell environment, there is more than one interfering cell. Some interfering BSs (intercell interference) are closer to the users in the desired cell and are likely to be dominant compared with the others. The other intercell interferers which have weaker strength are, in aggregate, defined as the remaining interference. Similar to [5], the remaining interference is treated as noise in this study.

2.1 Receiver architecture

The receiver applies postcoding vectors, $\boldsymbol{u}_{\alpha,i}$, to the received signal to cancel intercell interference producing the received symbol

$$\tilde{x}_{\alpha,i} = \boldsymbol{u}_{\alpha,i}^{*}\boldsymbol{y}_{\alpha,i}. \quad (4)$$

In [5], several receivers such as MF, MMSE and ZF receivers have been studied in the context of interference cancellation in multi-cell networks. It has been shown in [5] that ZF receivers require perfect CCSI and sufficient antennas to null all interference. This is not practical when many interfering sources are present in the network. The MF receiver is preferred when there are many unknown interferers without any CCSI [5]. MMSE receivers are superior when CCSI is available at the receivers [5]. Here, we assume that users are equipped with both MF and MMSE receivers, and use either of them depending on whether they are located in the cooperation zone as in Fig 1.

2.1.1 Non-cooperative users: Non-cooperative users utilise MF receivers due to the lack of CCSI. The postcoding vectors for MF receivers can be written as follows [5]

$$\boldsymbol{u}_{\alpha,i}^{\mathrm{MF}} = \max \text{ left singular vector of } (\boldsymbol{H}_{\alpha,i}). \quad (5)$$

2.1.2 Cooperative users: The users located in the cooperation zone have CCSI and thus are able to employ MMSE receivers which for user i in cell α are given by [5]

$$\boldsymbol{u}_{\alpha,i}^{\mathrm{MMSE}} = (\boldsymbol{\Psi}_{\alpha,i})^{-1}\boldsymbol{H}_{\alpha,i}\bar{\boldsymbol{P}}\boldsymbol{v}_{\alpha,i}, \quad (6)$$

© The Institution of Engineering and Technology 2016

where for the system considered here

$$\boldsymbol{\Psi}_{\alpha,i} = (1 + I_{\text{rem}})\boldsymbol{I}_{N_\text{r}} + \sum_{\beta} \frac{\rho_{\beta,i}}{K} \boldsymbol{G}_{\beta,i}\bar{\boldsymbol{P}}\boldsymbol{B}_\beta\boldsymbol{B}_\beta^*\bar{\boldsymbol{P}}^*\boldsymbol{G}_{\beta,i}^*, \tag{7}$$

where I_{rem} is the power of remaining interference and $\boldsymbol{B}_\beta = [\boldsymbol{v}_{\beta,1}, \ldots, \boldsymbol{v}_{\beta,K}]$ is a matrix containing out-of-cell precoders. In [5], it is assumed that the receivers average over the out-of-cell precoding vectors, due to the lack of actual out-of-cell precoder knowledge. Hence, the receivers do not use $\boldsymbol{B}_\beta\boldsymbol{B}_\beta^*$ but instead use

$$\mathbb{E}\left[\boldsymbol{B}_\beta\boldsymbol{B}_\beta^*\right] = \frac{1}{K + (N_\text{t} - K)\kappa^2}\begin{bmatrix} \boldsymbol{I}_K & \boldsymbol{0} \\ \boldsymbol{0} & \kappa^2\boldsymbol{I}_{N_\text{t}-K} \end{bmatrix}.$$

Therefore, we can rewrite (7) as follows

$$\boldsymbol{\Psi}_{\alpha,i} = (1 + I_{\text{rem}})\boldsymbol{I}_{N_\text{r}} + \sum_{\beta} \frac{\rho_{\beta,i}}{K + (N_\text{t} - K)\kappa^2} \boldsymbol{G}_{\beta,i}\bar{\boldsymbol{P}}\begin{bmatrix} \boldsymbol{I}_K & \boldsymbol{0} \\ \boldsymbol{0} & \kappa^2\boldsymbol{I}_{N_\text{t}-K} \end{bmatrix}\bar{\boldsymbol{P}}^*\boldsymbol{G}_{\beta,i}^*. \tag{8}$$

The value of $\mathbb{E}\left[\boldsymbol{B}_\beta\boldsymbol{B}_\beta^*\right]$ used in (8) is given in [5] for ZF precoders. Computing $\mathbb{E}\left[\boldsymbol{B}_\beta\boldsymbol{B}_\beta^*\right]$ with SLNR precoders involves the maximum eigenvector of a matrix. Hence, it is very difficult to derive a closed-form formula for the expectation for SLNR-based precoders. Via simulations, we find that the expectation for SLNR-based precoders also approximates that for ZF precoders, when the transmit SNR is high (interference limited region). The findings in [17, 18] also support our simulation results. Wang and Chen [17] indicates that regularised ZF (RZF) performs similarly to ZF precoders at high transmit SNR. Moreover, Yuan and Yang [18] shows that the SLNR precoder is equivalent to RZF. Therefore, considering our simulation results and the results in [17, 18], we use the expectation given in [5] for our SLNR-based precoders.

2.2 Transmitter architecture

The BS generates the precoders, $\boldsymbol{v}_{\alpha,\,i}$, based on the equivalent channels $\boldsymbol{u}_{\alpha,i}^*\boldsymbol{H}_{\alpha,i}\bar{\boldsymbol{P}}$ fed back by the users. We assume a perfect feedback link. Using precoders, intracell interference can be mitigated without any information required at the receiver side. In this paper, we consider ZF precoders and SLNR-based precoders.

2.2.1 ZF precoders: ZF precoders are computed by [16]

$$\begin{bmatrix} \boldsymbol{v}_{\alpha,1} & \boldsymbol{v}_{\alpha,2} & \cdots & \boldsymbol{v}_{\alpha,K} \end{bmatrix} = \boldsymbol{H}^*(\boldsymbol{H}\boldsymbol{H}^*)^{-1}, \tag{9}$$

where $\boldsymbol{H} = \left[\boldsymbol{u}_{\alpha,1}^*\boldsymbol{H}_{\alpha,1}\bar{\boldsymbol{P}}, \ldots, \boldsymbol{u}_{\alpha,K}^*\boldsymbol{H}_{\alpha,K}\bar{\boldsymbol{P}}\right]$. The precoders are then normalised, such that $\|\boldsymbol{v}_{\alpha,i}\|^2 = 1$.

2.2.2 SLNR-based precoders: In [8], the use of transmit precoding vectors based on the concept of signal leakage was proposed. The power of interference that is 'leaking' from the desired user i to user j is given by $|\sqrt{(\rho_{\alpha,j}/K)}\boldsymbol{u}_{\alpha,j}^*\boldsymbol{H}_{\alpha,j}\bar{\boldsymbol{P}}\boldsymbol{v}_{\alpha,i}|^2$. The SLNR parameter for user i is thus given by

$$\text{SLNR}_i = \frac{(\rho_{\alpha,i}/K)\boldsymbol{v}_{\alpha,i}^*\bar{\boldsymbol{P}}^*\boldsymbol{H}_{\alpha,i}^*\boldsymbol{u}_{\alpha,i}\boldsymbol{u}_{\alpha,i}^*\boldsymbol{H}_{\alpha,i}\bar{\boldsymbol{P}}\boldsymbol{v}_{\alpha,i}}{1 + \boldsymbol{v}_{\alpha,i}^*\tilde{\boldsymbol{H}}_{\alpha,i}^*\tilde{\boldsymbol{H}}_{\alpha,i}\boldsymbol{v}_{\alpha,i}}, \tag{10}$$

where

$$\tilde{\boldsymbol{H}}_{\alpha,i} = \begin{bmatrix} \boldsymbol{F}_{\alpha,1}^\text{T} & \boldsymbol{F}_{\alpha,2}^\text{T} & \cdots & \boldsymbol{F}_{\alpha,i-1}^\text{T} & \boldsymbol{F}_{\alpha,i+1}^\text{T} & \cdots & \boldsymbol{F}_{\alpha,K}^\text{T} \end{bmatrix}^\text{T} \text{ and}$$

$$\boldsymbol{F}_{\alpha,i} = \sqrt{(\rho_{\alpha,i}/K)}\boldsymbol{u}_{\alpha,i}^*\boldsymbol{H}_{\alpha,i}\bar{\boldsymbol{P}}. \tag{11}$$

$\tilde{\boldsymbol{H}}_{\alpha,i}$ is an extended equivalent channel which excludes the desired equivalent channel $\boldsymbol{u}_{\alpha,i}^*\boldsymbol{H}_{\alpha,i}\bar{\boldsymbol{P}}$. We select precoding vectors, $\boldsymbol{v}_{\alpha,i}$, $i = \{1, 2, 3, \ldots, K\}$, such that (10) is maximised over $\boldsymbol{v}_{\alpha,i}$, subject to $\|\boldsymbol{v}_{\alpha,i}\|^2 = 1$. Using the Rayleigh quotient as shown in [19] we find the vector, $\boldsymbol{v}_{\alpha,i}$, which maximises the SLNR as the leading eigenvector of $\left(\boldsymbol{I} + (\tilde{\boldsymbol{H}}_{\alpha,i}^*\tilde{\boldsymbol{H}}_{\alpha,i})\right)^{-1}(\rho_{\alpha,i}/K)\bar{\boldsymbol{P}}^*\boldsymbol{H}_{\alpha,i}^*\boldsymbol{u}_{\alpha,i}\boldsymbol{u}_{\alpha,i}^*\boldsymbol{H}_{\alpha,i}\bar{\boldsymbol{P}}$.

2.3 Algorithm

We now describe the algorithm for the proposed cooperative interference cancellation scheme.

- *Decision of cooperation:* The users decide on cooperation based on the ratio of channel strengths

$$r_\beta = 10\log_{10}\left(\frac{\text{tr}(\boldsymbol{H}_{\alpha,i}\boldsymbol{H}_{\alpha,i}^*)}{\text{tr}(\boldsymbol{G}_{\beta,i}\boldsymbol{G}_{\beta,i}^*)}\right). \tag{12}$$

We set a threshold, Λ. If $r_\beta > \Lambda$, then the user is in a no-cooperation zone and it activates the MF receiver. If $r_\beta < \Lambda$, then the user is in a cooperation zone, receives CCSI from neighbouring BS(s), and activates the MMSE receiver. If all users are in the cooperation zone, we refer to this case as full cooperation. If some users are in the no-cooperation zone, then this is referred to as partial cooperation.

- *Generating postcoding vectors*: Each user generates its postcoding vector according to their designations:
  - *Cooperative users:* MMSE postcoders need precoders as given in (6). Both ZF and SLNR precoders also need postcoders (see (9) and (10)). Therefore, the cooperative users first initialise their postcoders as follows

$$\boldsymbol{u}_{\alpha,i}^{(0)} = (\boldsymbol{\Psi}_{\alpha,i})^{-1}\boldsymbol{H}_{\alpha,i}\bar{\boldsymbol{P}}\boldsymbol{v}_{\alpha,i}^{(0)}, \tag{13}$$

where we set $\boldsymbol{v}_{\alpha,i}^{(0)}$ as the maximum eigenvector of $\bar{\boldsymbol{P}}^*\boldsymbol{H}_{\alpha,i}^*\boldsymbol{\Psi}_{\alpha,i}^{-1}\boldsymbol{H}_{\alpha,i}\bar{\boldsymbol{P}}$.
  - *Non-cooperative users:* Non-cooperative users activate the MF receiver which does not need any initialisation because the MF receiver does not require the precoding vectors. We generate non-cooperative users' postcoding vectors using (5).
- *Generating precoding vectors:* Depending on the precoding type, the BS computes the precoding vectors.
  - ZF precoders

$$\begin{bmatrix} \boldsymbol{v}_{\alpha,1}^{(1)} & \boldsymbol{v}_{\alpha,2}^{(1)} & \cdots & \boldsymbol{v}_{\alpha,k}^{(1)} \end{bmatrix} = \boldsymbol{H}^{(\boldsymbol{0})*}(\boldsymbol{H}^{(\boldsymbol{0})}\boldsymbol{H}^{(\boldsymbol{0})*})^{-1}, \tag{14}$$

where $\boldsymbol{H}^{(0)} = \left[\boldsymbol{u}_{\alpha,1}^{(0)*}\boldsymbol{H}_{\alpha,1}\bar{\boldsymbol{P}}, \ldots, \boldsymbol{u}_{\alpha,K}^{(0)*}\boldsymbol{H}_{\alpha,K}\bar{\boldsymbol{P}}\right]$.
  - *SLNR precoders* $\boldsymbol{v}_{\alpha,i}^{(1)}$, is the leading eigenvector of $\left(\boldsymbol{I} + \tilde{\boldsymbol{H}}_{\alpha,i}^{(0)*}\tilde{\boldsymbol{H}}_{\alpha,i}^{(0)}\right)^{-1}(\rho_{\alpha,i}/K)\bar{\boldsymbol{P}}^*\boldsymbol{H}_{\alpha,i}^*\boldsymbol{u}_{\alpha,i}^{(0)}\boldsymbol{u}_{\alpha,i}^{(0)*}\boldsymbol{H}_{\alpha,i}\bar{\boldsymbol{P}}$, where

$$\tilde{\boldsymbol{H}}_{\alpha,i}^{(0)} = \begin{bmatrix} \boldsymbol{F}_{\alpha,1}^{(0)\text{T}} & \boldsymbol{F}_{\alpha,2}^{(0)\text{T}} & \cdots & \boldsymbol{F}_{\alpha,i-1}^{(0)\text{T}} & \boldsymbol{F}_{\alpha,i+1}^{(0)\text{T}} & \cdots & \boldsymbol{F}_{\alpha,K}^{(0)\text{T}} \end{bmatrix}^\text{T} \text{ and}$$

$$\boldsymbol{F}_{\alpha,i}^{(0)} = \sqrt{\frac{\rho_{\alpha,i}}{K}}\boldsymbol{u}_{\alpha,i}^{(0)*}\boldsymbol{H}_{\alpha,i}\bar{\boldsymbol{P}}. \tag{15}$$

and then the BS use the precoders generated. In [5], iteration between the BS and the users was applied to update the postcoders and precoders. However, we do not use iteration in this work as it would increase the overhead dramatically.

Table 1 Summary of the system

	Precoder	Postcoder
cooperative users	ZF/SLNR	MMSE
non-cooperative users	ZF/SLNR	MF

© The Institution of Engineering and Technology 2016

Finally, we can summarise the system to give the precoders and postcoders for cooperative and non-cooperative users in Table 1.

3 Performance metrics

We consider three metrics to analyse the system performance: the signal-to-interference noise ratio (SINR), the cooperation gain and mean sum rates.

(i) For the system described, the SINR for user i in cell α is defined as

$$\mathrm{SINR}_{\alpha,i} = \frac{(\rho_{\alpha,i}/K)\boldsymbol{u}_{\alpha,i}^{*}\boldsymbol{H}_{\alpha,i}\bar{\boldsymbol{P}}\boldsymbol{v}_{\alpha,i}\boldsymbol{v}_{\alpha,i}^{*}\bar{\boldsymbol{P}}^{*}\boldsymbol{H}_{\alpha,i}^{*}\boldsymbol{u}_{\alpha,i}}{1 + I_{\mathrm{rem}} + \Delta_{\alpha,i} + \Omega_{\alpha,i}}, \tag{16}$$

where $\Delta_{\alpha,i}$ is the intracell interference defined as

$$\Delta_{\alpha,i} = \left(\frac{\rho_{\alpha,i}}{K}\right)\sum_{k=1,i\neq k}^{K}\boldsymbol{u}_{\alpha,i}^{*}\boldsymbol{H}_{\alpha,i}\bar{\boldsymbol{P}}\boldsymbol{v}_{\alpha,k}\boldsymbol{v}_{\alpha,k}^{*}\bar{\boldsymbol{P}}^{*}\boldsymbol{H}_{\alpha,i}^{*}\boldsymbol{u}_{\alpha,i}. \tag{17}$$

In (16), $\Omega_{\alpha,i}$ is the power of intercell interference from neighbouring cells, indexed by β, to cell α and is given by

$$\Omega_{\alpha,i} = \sum_{\beta}\left(\frac{\rho_{\beta,i}}{K}\right)\sum_{k=1}^{K}\boldsymbol{u}_{\alpha,i}^{*}\boldsymbol{G}_{\beta,i}\bar{\boldsymbol{P}}\boldsymbol{v}_{\beta,k}\boldsymbol{v}_{\beta,k}^{*}\bar{\boldsymbol{P}}^{*}\boldsymbol{G}_{\beta,i}^{*}\boldsymbol{u}_{\alpha,i}. \tag{18}$$

(ii) The cooperation gain is defined as

$$\phi = \mathbb{E}\left\{\frac{\mathrm{SINR}_{\alpha,i}^{\text{cooperation}}}{\mathrm{SINR}_{\alpha,i}^{\text{no-cooperation}}}\right\}. \tag{19}$$

$\mathrm{SINR}_{\alpha,i}^{\text{cooperation}}$ is the SINR achieved by the described cooperation scheme, while $\mathrm{SINR}_{\alpha,i}^{\text{no-cooperation}}$ represents the benchmark SINR where the system does not permit cooperation for *any* users.

(iii) The mean sum rate per unit bandwidth for cell α is given by

$$R_{\alpha} = \mathbb{E}\left\{\sum_{i=1}^{K}\log_2\left(1 + \mathrm{SINR}_{\alpha,i}\right)\right\}. \tag{20}$$

(iv) Finally the outage probability for user i in cell α is given by

$$p_{\alpha,i}^{\text{out}}(R_{\tau}) = \mathbb{P}\{\log_2\left(1 + \mathrm{SINR}_{\alpha,i}\right) < R_{\tau}\}, \tag{21}$$

where R_{τ} is the chosen rate threshold. In this paper, we assume that the users with received SINR less than −5 dB are in outage, that is, $R_{\tau} = \log_2(1 + 10^{-0.5}) = 0.3964$.

3.1 Imperfect cross channel state information

3.1.1 Imperfect channel model: [Note that we assume the desired channel, $\boldsymbol{H}_{\alpha,i}$, is perfectly known because it is reasonable that the user can obtain its own desired channel information with a high degree of accuracy.] By considering CCSI imperfections, we examine the effective miscancellation of intercell interference by the MMSE receivers. Erroneous cross channel matrices are denoted as $\hat{\boldsymbol{G}}_{\beta,k}$ and modelled by [16]

$$\hat{\boldsymbol{G}}_{\beta,i} = \varsigma\boldsymbol{G}_{\beta,i} + \bar{\varsigma}\,\boldsymbol{\Pi}_{\beta,i}, \tag{22}$$

where ς, $0 \leq \varsigma \leq 1$ and $\bar{\varsigma} = \sqrt{1-\varsigma^2}$, control the amount of CCSI imperfection (i.e. $\varsigma = 1$ refers to perfect CCSI) and $\boldsymbol{\Pi}_{\beta,i}$ is an $(N_{\mathrm{r}} \times N_{\mathrm{t}})$ complex Gaussian matrix with zero mean and unit variance. It is shown in [20, 21] that ς can be used to determine the impact of several factors on imperfect CCSI and can be a function of the length of the training sequence, SNR and Doppler frequency.

3.1.2 Instantaneous intercell interference with imperfect CCSI: Imperfect channel estimation causes miscancellation of intercell interference and thus leads to additional interference. We can represent the instantaneous intercell interference with imperfect CCSI, $\hat{\Omega}_{\alpha,i}$, as follows

$$\hat{\Omega}_{\alpha,i} = \Omega_{\alpha,i} + \tilde{\Omega}_{\alpha,i}, \tag{23}$$

where $\tilde{\Omega}_{\alpha,i}$ is the additional interference caused by imperfect CCSI. We first write the erroneous postcoding vectors for users in the overlapping regions by replacing $\boldsymbol{G}_{\beta,i}$ with $\hat{\boldsymbol{G}}_{\beta,i}$ in (7). This gives

$$\hat{\boldsymbol{u}}_{\alpha,i}^{\mathrm{MMSE}} = (\hat{\boldsymbol{\Psi}}_{\alpha,i})^{-1}\boldsymbol{H}_{\alpha,i}\bar{\boldsymbol{P}}\boldsymbol{v}_{\alpha,i}, \tag{24}$$

where the erroneous covariance matrix is

$$\hat{\boldsymbol{\Psi}}_{\alpha,i} = (1 + I_{\mathrm{rem}})\boldsymbol{I}_{N_{\mathrm{r}}} + \sum_{\beta}\frac{\rho_{\beta,i}}{K + (N_{\mathrm{t}} - K)\kappa^2} \times \hat{\boldsymbol{G}}_{\beta,i}\bar{\boldsymbol{P}}\begin{bmatrix}\boldsymbol{I}_K & \boldsymbol{0}\\ \boldsymbol{0} & \kappa^2\boldsymbol{I}_{N_{\mathrm{t}}-K}\end{bmatrix}\bar{\boldsymbol{P}}^{*}\hat{\boldsymbol{G}}_{\beta,i}^{*}. \tag{25}$$

Substituting (22) into (25), we obtain (see (26))

We can rewrite (26) as follows

$$\hat{\boldsymbol{\Psi}}_{\alpha,i} = \boldsymbol{\Psi}_{\alpha,i} + \boldsymbol{T}_{\alpha,i}, \tag{27}$$

where (see (28))

We drop the superscript of MMSE in (24) for notational clarity and write the intercell interference term as follows

$$\hat{\Omega}_{\alpha,i} = \sum_{\beta}\left(\frac{\rho_{\beta,i}}{K}\right)\sum_{k=1}^{K}\hat{\boldsymbol{u}}_{\alpha,i}^{*}\boldsymbol{G}_{\beta,i}\bar{\boldsymbol{P}}\boldsymbol{v}_{\beta,k}\boldsymbol{v}_{\beta,k}^{*}\bar{\boldsymbol{P}}^{*}\boldsymbol{G}_{\beta,i}^{*}\hat{\boldsymbol{u}}_{\alpha,i}. \tag{29}$$

Substituting (24) and (27) into (29), (see equation (30) at the bottom of the next page)

To find the instantaneous interference term with imperfect CCSI, we need to find the inverse of the erroneous covariance matrix $\hat{\boldsymbol{\Psi}}_{\alpha,i}^{-1}$ in

$$\hat{\boldsymbol{\Psi}}_{\alpha,i} = (1 + I_{\mathrm{rem}})\boldsymbol{I}_{N_{\mathrm{r}}} + \sum_{\beta}\frac{\rho_{\beta,i}}{K + (N_{\mathrm{t}} - K)\kappa^2}(\varsigma\boldsymbol{G}_{\beta,i} + \bar{\varsigma}\,\boldsymbol{\Pi}_{\beta,i})\bar{\boldsymbol{P}}\begin{bmatrix}\boldsymbol{I}_K & \boldsymbol{0}\\ \boldsymbol{0} & \kappa^2\boldsymbol{I}_{N_{\mathrm{t}}-K}\end{bmatrix}\bar{\boldsymbol{P}}^{*}(\varsigma\boldsymbol{G}_{\beta,i} + \bar{\varsigma}\,\boldsymbol{\Pi}_{\beta,i})^{*}. \tag{26}$$

$$\begin{aligned}\boldsymbol{T}_{\alpha,i} = \sum_{\beta}\frac{\rho_{\beta,i}}{K + (N_{\mathrm{t}} - K)\kappa^2}\Bigg(&\left((\varsigma^2 - 1)\boldsymbol{G}_{\beta,i}\bar{\boldsymbol{P}}\begin{bmatrix}\boldsymbol{I}_K & \boldsymbol{0}\\ \boldsymbol{0} & \kappa^2\boldsymbol{I}_{N_{\mathrm{t}}-K}\end{bmatrix}\bar{\boldsymbol{P}}^{*}\boldsymbol{G}_{\beta,i}^{*}\right) + \left(\varsigma\bar{\varsigma}\boldsymbol{G}_{\beta,i}\bar{\boldsymbol{P}}\begin{bmatrix}\boldsymbol{I}_K & \boldsymbol{0}\\ & \boldsymbol{0}\kappa^2\boldsymbol{I}_{N_{\mathrm{t}}-K}\end{bmatrix}\bar{\boldsymbol{P}}^{*}\boldsymbol{\Pi}_{\beta,i}^{*}\right)\\ &+\left(\varsigma\bar{\varsigma}\,\boldsymbol{\Pi}_{\beta,i}\bar{\boldsymbol{P}}\begin{bmatrix}\boldsymbol{I}_K & \boldsymbol{0}\\ \boldsymbol{0} & \kappa^2\boldsymbol{I}_{N_{\mathrm{t}}-K}\end{bmatrix}\bar{\boldsymbol{P}}^{*}\boldsymbol{G}_{\beta,i}^{*}\right)+\left(\bar{\varsigma}^2\boldsymbol{\Pi}_{\beta,i}\bar{\boldsymbol{P}}\begin{bmatrix}\boldsymbol{I}_K & \boldsymbol{0}\\ \boldsymbol{0} & \kappa^2\boldsymbol{I}_{N_{\mathrm{t}}-K}\end{bmatrix}\bar{\boldsymbol{P}}^{*}\boldsymbol{\Pi}_{\beta,i}^{*}\right)\Bigg).\end{aligned} \tag{28}$$

IET Commun., 2016, Vol. 10, Iss. 5, pp. 525–533
© The Institution of Engineering and Technology 2016

(30) which involves the inverse of the summation of two full rank matrices as in (27), where the second matrix ($\boldsymbol{T}_{\alpha,i}$) includes information about imperfect CCSI as given in (28). Taking the inverse of (27) is not straightforward. In [22], the authors provide a recursive solution for the inverse of a summation of two non-singular matrix which is applicable to our system.

• *Result 1:* $\boldsymbol{\Psi}_{\alpha,i}$ and $\boldsymbol{\Psi}_{\alpha,i}+\boldsymbol{T}_{\alpha,i}$ are non-singular matrices. $\boldsymbol{T}_{\alpha,i}$ (with positive rank) can be decomposed into matrices of rank 1 [22], $\boldsymbol{T}_{\alpha,i}=\Upsilon_1+\Upsilon_2+\ldots+\Upsilon_{\text{rank}(\boldsymbol{T}_{\alpha,i})}$, where Υ_k is simply a matrix in which the kth column is the kth column of $\boldsymbol{T}_{\alpha,i}$ and other elements are zero. Let $\boldsymbol{C}_{k+1}=\boldsymbol{\Psi}_{\alpha,i}+\Upsilon_1+\ldots+\Upsilon_k$, where $k=1,\ \ldots,$ rank ($\boldsymbol{T}_{\alpha,i}$). Then if $\boldsymbol{C}_1=\boldsymbol{\Psi}_{\alpha,i}$,

$$\hat{\boldsymbol{\Psi}}_{\alpha,i}^{-1}=\left(\boldsymbol{\Psi}_{\alpha,i}+\boldsymbol{T}_{\alpha,i}\right)^{-1}=\boldsymbol{\Psi}_{\alpha,i}^{-1}-\sum_{k=1}^{\text{rank}(\boldsymbol{T}_{\alpha,i})}\nu_k\boldsymbol{C}_k^{-1}\Upsilon_k\boldsymbol{C}_k^{-1},\quad(31)$$

where

$$\nu_k=\frac{1}{1+\text{tr}(\boldsymbol{C}_k^{-1}\Upsilon_k)}.$$

Proof: We first write $\boldsymbol{C}_2=\boldsymbol{C}_1+\Upsilon_1$ and recall that $\boldsymbol{\Psi}_{\alpha,i}$ and $\boldsymbol{C}_2$ are non-singular. Using lemma in [22]

$$\boldsymbol{C}_2^{-1}=\boldsymbol{\Psi}_{\alpha,i}^{-1}-\nu_1\boldsymbol{\Psi}_{\alpha,i}^{-1}\Upsilon_1\boldsymbol{\Psi}_{\alpha,i}^{-1},\quad(32)$$

and we have calculated $\boldsymbol{C}_2$ in terms of $\boldsymbol{\Psi}_{\alpha,i}^{-1}$. Now let us write $\boldsymbol{C}_3=\boldsymbol{\Psi}_{\alpha,i}+\Upsilon_1+\Upsilon_2=\boldsymbol{C}_2+\Upsilon_2$. Hence, since $\boldsymbol{C}_2$ and $\boldsymbol{C}_3$ are non-singular, we may again use the lemma in [22] and find

$$\boldsymbol{C}_3^{-1}=\boldsymbol{C}_2^{-1}-\nu_2\boldsymbol{C}_2^{-1}\Upsilon_2\boldsymbol{C}_2^{-1}.\quad(33)$$

$\boldsymbol{C}_2^{-1}$ is found by (32). Substituting (32) into (33)

$$\boldsymbol{C}_3^{-1}=\boldsymbol{\Psi}_{\alpha,i}^{-1}-\nu_1\boldsymbol{\Psi}_{\alpha,i}^{-1}\Upsilon_1\boldsymbol{\Psi}_{\alpha,i}^{-1}-\nu_2\boldsymbol{C}_2^{-1}\Upsilon_2\boldsymbol{C}_2^{-1}.\quad(34)$$

Repeating this process rank($\boldsymbol{T}_{\alpha,i}$) times, we obtain

$$\boldsymbol{C}_{\text{rank}(\boldsymbol{T}_{\alpha,i})+1}^{-1}=\boldsymbol{\Psi}_{\alpha,i}^{-1}-\sum_{k=1}^{\text{rank}(\boldsymbol{T}_{\alpha,i})}\nu_k\boldsymbol{C}_k^{-1}\Upsilon_k\boldsymbol{C}_k^{-1}.\quad(35)$$

Noting that $\boldsymbol{C}_{\text{rank}(\boldsymbol{T}_{\alpha,i})}+1=(\boldsymbol{\Psi}_{\alpha,i}+\boldsymbol{T}_{\alpha,i})$ proves our result.

Using (31), the instantaneous intercell interference with imperfect CCSI is given by (see (36))
The additional interference caused by imperfect CCSI, $\tilde{\Omega}_{\alpha,i}$, can be given as follows

$$\tilde{\Omega}_{\alpha,i}=\hat{\Omega}_{\alpha,i}-\Omega_{\alpha,i}.\quad(37)$$

Substituting (36) and (18) into (37) (see (38))

where

$$\boldsymbol{D}_{\alpha,i}=\sum\nolimits_{\beta}\left(\frac{\rho_{\beta,i}}{K}\right)\sum\nolimits_{k=1}^{K}\boldsymbol{G}_{\beta,i}\bar{\boldsymbol{P}}\boldsymbol{v}_{\beta,k}\boldsymbol{v}_{\beta,k}^{*}\bar{\boldsymbol{P}}^{*}\boldsymbol{G}_{\beta,i}^{*}.$$

Main motivation to find (38) is to find the expected value of the additional interference. However, because (38) is such a complex expression, it is very hard to find the expected value. Therefore, we only give the instantaneous additional interference as in (38).

4 Simulation results

4.1 Environments

We analyse our scheme in a hexagonal array of 19 cells where we generate random user locations. In the simulations, we use the COST 231 Hata model and consider the three-sector antenna pattern given in [23]. We also consider log-normal shadowing with 8 dB standard deviation. Other parameters are as follows

- *Tx* Power = 46 dBm;
- *Tx* Antenna Gain = 14 dBi;
- *Rx* Antenna Gain = 0 dBi;
- *Rx* noise figure (NF) = 9 dB;
- the carrier frequency f_c = 1.9 GHz;
- bandwidth = 10 MHz.

In our 3GPP urban macro cell simulations we calculate the received $\overline{\text{SNR}}=\left(\rho_{\alpha,i}/\sigma^2\right)$, where $\rho_{\alpha,i}$ is the desired signal power at the receiver, σ^2 is the noise variance found using the parameters as above and in [23]. Similarly we define the $\overline{\text{INR}}=(\rho_{\beta,i}/\sigma^2)$. We also calculate the received $\overline{\text{SINR}}=(\rho_{\alpha,i}/\sum_{\beta}\sum_{a=1}^{3}\rho_{\beta,i}^{(a)}+\sigma^2)$ where $\rho_{\beta,i}^{(a)}$ is the long term interference power from the βth BS and the ath sector. Note that the bar notation is used to denote the fact that the expression is a long-term SINR, different from the instantenous SINR given in (16). We assume 19 cells with three sectors, therefore the total intercell interference is generated by 56 sectors, excluding the desired sector.

4.1.1 Urban areas: In [23], the path loss for urban areas is given. Assuming the intersite distance is 2 km, we calculate $\overline{\text{SINR}}$ and $\overline{\text{INR}}$.

In Fig. 2*a*, we give $\overline{\text{SNR}}$ and $\overline{\text{SINR}}$ results. We also calculate the $\overline{\text{SINR}}$ by removing the strongest two interferers, to show the gain that can be achieved by intercell interference cancellation. It can

$$\begin{aligned}\hat{\Omega}_{\alpha,i}&=(\hat{\boldsymbol{\Psi}}_{\alpha,i}^{-1}\boldsymbol{H}_{\alpha,i}\bar{\boldsymbol{P}}\boldsymbol{v}_{\alpha,i})^{*}\sum_{\beta}\left(\frac{\rho_{\beta,i}}{K}\right)\sum_{k=1}^{K}\boldsymbol{G}_{\beta,i}\bar{\boldsymbol{P}}\boldsymbol{v}_{\beta,k}\boldsymbol{v}_{\beta,k}^{*}\bar{\boldsymbol{P}}^{*}\boldsymbol{G}_{\beta,i}^{*}(\hat{\boldsymbol{\Psi}}_{\alpha,i}^{-1}\boldsymbol{H}_{\alpha,i}\boldsymbol{v}_{\alpha,i})\\&=\left((\boldsymbol{\Psi}_{\alpha,i}+\boldsymbol{T}_{\alpha,i})^{-1}\boldsymbol{H}_{\alpha,i}\bar{\boldsymbol{P}}\boldsymbol{v}_{\alpha,i}\right)^{*}\sum_{\beta}\left(\frac{\rho_{\beta,i}}{K}\right)\sum_{k=1}^{K}\boldsymbol{G}_{\beta,i}\bar{\boldsymbol{P}}\boldsymbol{v}_{\beta,k}\boldsymbol{v}_{\beta,k}^{*}\bar{\boldsymbol{P}}^{*}\boldsymbol{G}_{\beta,i}^{*}\left((\boldsymbol{\Psi}_{\alpha,i}+\boldsymbol{T}_{\alpha,i})^{-1}\boldsymbol{H}_{\alpha,i}\bar{\boldsymbol{P}}\boldsymbol{v}_{\alpha,i}\right).\end{aligned}\quad(30)$$

$$\hat{\Omega}_{\alpha,i}=\left(\left(\boldsymbol{\Psi}_{\alpha,i}^{-1}-\sum_{k=1}^{\text{rank}(\boldsymbol{T}_{\alpha,i})}\nu_k\boldsymbol{C}_k^{-1}\Upsilon_k\boldsymbol{C}_k^{-1}\right)\boldsymbol{H}_{\alpha,i}\bar{\boldsymbol{P}}\boldsymbol{v}_{\alpha,i}\right)^{*}\sum_{\beta}\left(\frac{\rho_{\beta,i}}{K}\right)\sum_{k=1}^{K}\boldsymbol{G}_{\beta,i}\bar{\boldsymbol{P}}\boldsymbol{v}_{\beta,k}\boldsymbol{v}_{\beta,k}^{*}\bar{\boldsymbol{P}}^{*}\boldsymbol{G}_{\beta,i}^{*}\left(\left(\boldsymbol{\Psi}_{\alpha,i}^{-1}-\sum_{k=1}^{\text{rank}(\boldsymbol{T}_{\alpha,i})}\nu_k\boldsymbol{C}_k^{-1}\Upsilon_k\boldsymbol{C}_k^{-1}\right)\boldsymbol{H}_{\alpha,i}\bar{\boldsymbol{P}}\boldsymbol{v}_{\alpha,i}\right).\quad(36)$$

$$\begin{aligned}\tilde{\Omega}_{\alpha,i}=&\left(\left(\sum_{k=1}^{\text{rank}(\boldsymbol{T}_{\alpha,i})}\nu_k\boldsymbol{C}_k^{-1}\Upsilon_k\boldsymbol{C}_k^{-1}\right)\boldsymbol{H}_{\alpha,i}\bar{\boldsymbol{P}}\boldsymbol{v}_{\alpha,i}\right)^{*}\boldsymbol{D}_{\alpha,i}\left(\left(\sum_{k=1}^{\text{rank}(\boldsymbol{T}_{\alpha,i})}\nu_k\boldsymbol{C}_k^{-1}\Upsilon_k\boldsymbol{C}_k^{-1}\right)\boldsymbol{H}_{\alpha,i}\bar{\boldsymbol{P}}\boldsymbol{v}_{\alpha,i}\right)\\&-\left(\boldsymbol{\Psi}_{\alpha,i}^{-1}\boldsymbol{H}_{\alpha,i}\bar{\boldsymbol{P}}\boldsymbol{v}_{\alpha,i}\right)^{*}\boldsymbol{D}_{\alpha,i}\left(\left(\sum_{k=1}^{\text{rank}(\boldsymbol{T}_{\alpha,i})}\nu_k\boldsymbol{C}_k^{-1}\Upsilon_k\boldsymbol{C}_k^{-1}\right)\boldsymbol{H}_{\alpha,i}\bar{\boldsymbol{P}}\boldsymbol{v}_{\alpha,i}\right)-\left(\left(\sum_{k=1}^{\text{rank}(\boldsymbol{T}_{\alpha,i})}\nu_k\boldsymbol{C}_k^{-1}\Upsilon_k\boldsymbol{C}_k^{-1}\right)\boldsymbol{H}_{\alpha,i}\bar{\boldsymbol{P}}\boldsymbol{v}_{\alpha,i}\right)^{*}\boldsymbol{D}_{\alpha,i}\left(\boldsymbol{\Psi}_{\alpha,i}^{-1}\boldsymbol{H}_{\alpha,i}\bar{\boldsymbol{P}}\boldsymbol{v}_{\alpha,i}\right),\end{aligned}\quad(38)$$

© The Institution of Engineering and Technology 2016

be seen in Fig. 2*a* that the total interference causes a 19 dB loss at the median cdf point. If we cancel the strongest two interferers, this loss decreases to approximately 12 dB. The uncancelled interferers result in remaining interference. Fig. 2*b* shows the $\bar{\text{INR}}$ of each interfering sector, ordered from maximum to minimum. The first two interfering sectors are more dominant than the others, however the total remaining interference is still significantly high. Considering the existence of two dominant interferers, we find $\gamma = \left(\bar{\text{INR}}_{\text{rem}}/\bar{\text{INR}}_{\text{dom}}\right) \simeq 0.68$ on average for randomly located users.

Overlapping region for urban areas: Assuming the users are uniformly located, if we set $\Lambda = 8$ dB, we find that the overlapping region with only one adjacent cell consists of approximately 17% of all users via simulations. We also find that the overlapping region with two adjacent cells consists of approximately 31% of all users via simulations.

4.1.2 Suburban areas: The path loss for suburban areas is given in [23], which is 3 dB less than the corresponding path loss for urban users. Assuming that the intersite distance is 4 km, we calculate $\bar{\text{SINR}}$ and $\bar{\text{INR}}$ for suburban areas and the results are given in Fig. 3.

As seen in Fig. 3*a*, there is approximately a 12 dB loss at the median cdf point, caused by interference. This loss descreases to approximately 5 dB if we can cancel the two strongest interferers. Even though the loss caused by interference is less than the corresponding value for urban users, the $\bar{\text{SINR}}$ of suburban users is similar to that of the urban users due to the increased path loss caused by a longer intersite distance. As seen in Fig. 3*b*, there are two interferers significantly stronger than the remaining interference, however, due to path loss, suburban interference powers are less than urban interference powers. Considering the existence of two dominant interferers, we find $\gamma \simeq 0.62$ on average for randomly located users in suburban environments.

Overlapping region for suburban areas: If we set $\Lambda = 8$ dB in the simulations, we observe in the simulations that the overlapping region with only one adjacent cell consists of approximately 16% of all users. We also observe that the overlapping region with two adjacent cells consists of approximately 30% of all users in the simulations.

4.2 Performance comparisons

Here we give simulation results of our cooperative scheme. We consider $K = 3$ users in each cell, equipped with $N_r = 4$ antennas. We also assume that the BS is equipped with $N_t = 4$ antennas.

4.2.1 Urban area performance comparisons: We first evaluate the simulations for users in urban areas. We give mean sum rates using (20) for these users in Fig. 4. We compare SLNR precoders with ZF Precoders for no-cooperation, full cooperation

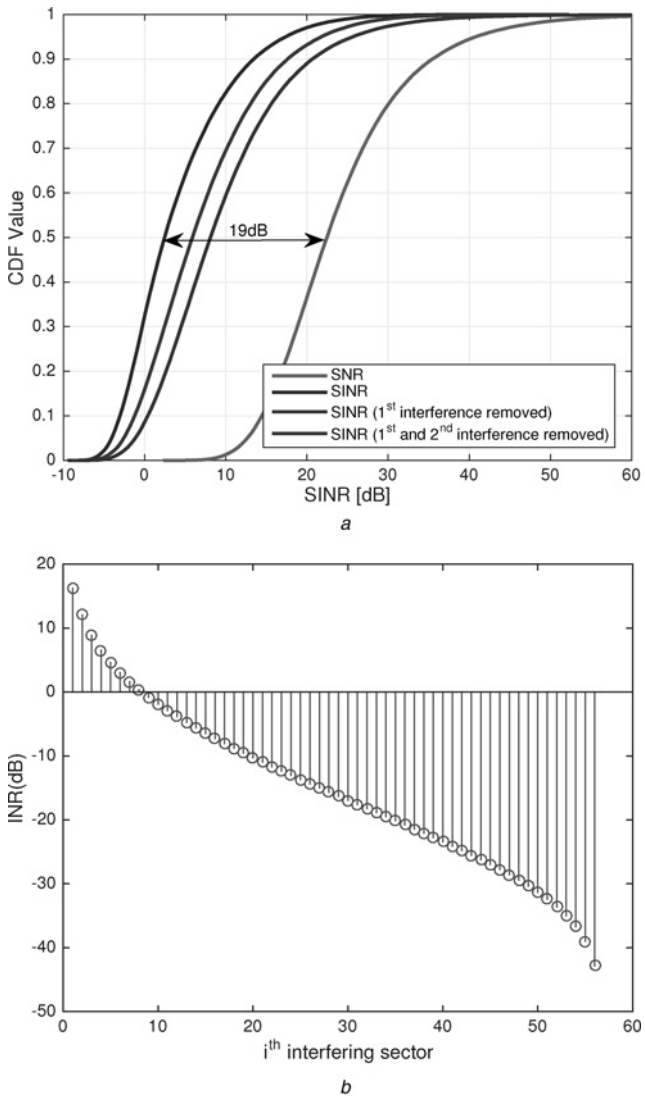

Fig. 2 *Received $\bar{\text{SINR}}$ and $\bar{\text{INR}}$ for urban area*
a Received $\bar{\text{SNR}}$ and $\bar{\text{SINR}}$
b $\bar{\text{INR}}$

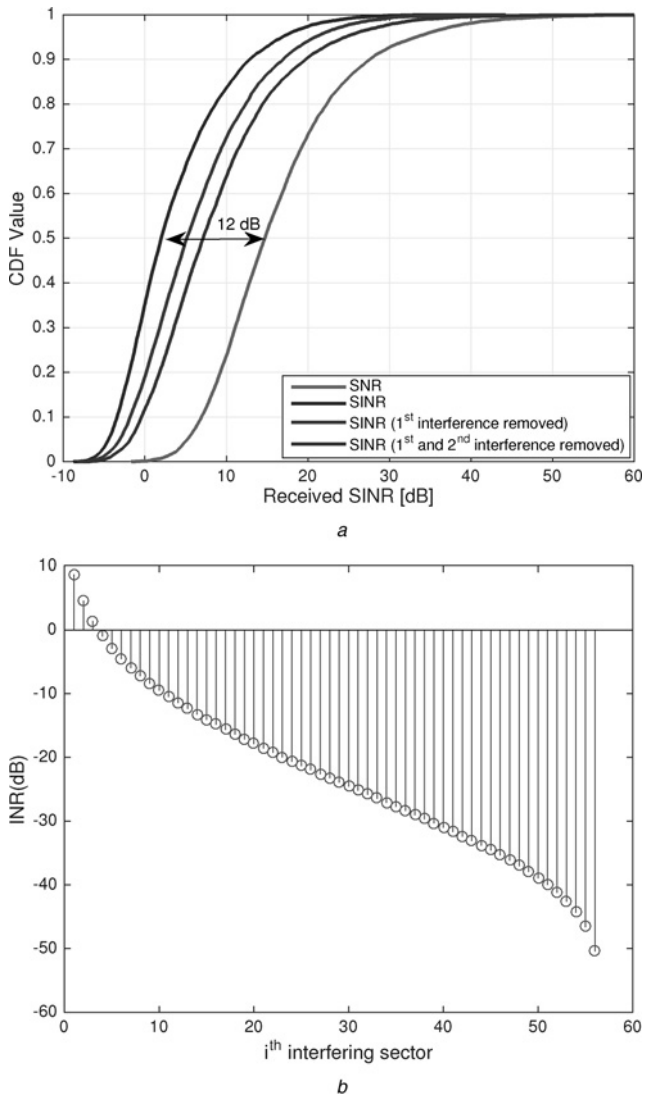

Fig. 3 *Received $\bar{\text{SINR}}$ and $\bar{\text{INR}}$ for suburban area*
a Received $\bar{\text{SNR}}$ and $\bar{\text{SINR}}$
b $\bar{\text{INR}}$

IET Commun., 2016, Vol. 10, Iss. 5, pp. 525–533
© The Institution of Engineering and Technology 2016

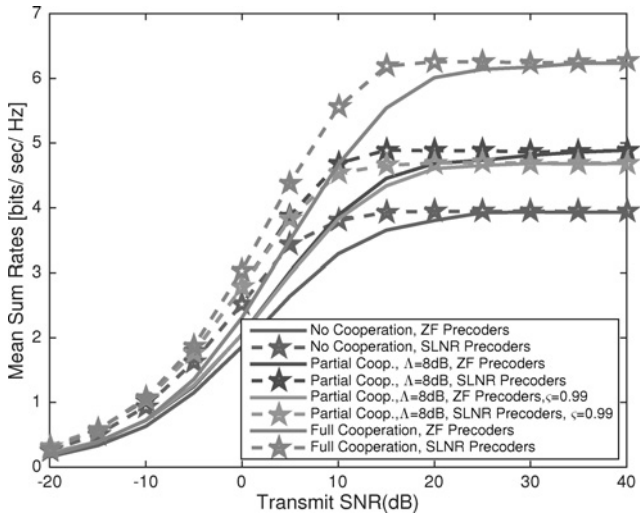

Fig. 4 *Mean sum rates for urban users*

and partial cooperation schemes. For partial cooperation, we assume $\Lambda = 8$ dB as mentioned in Section 4.1.

As seen in Fig. 4, SLNR precoders provide better sum rates than ZF precoders from very low transmit SNRs up to 25 dB. After this value, the performance of SLNR precoders approaches ZF precoders. The simulation results also indicate that full cooperation can increase the mean sum rate by approximately 55% compared with the no-cooperation scheme. On the other hand, setting $\Lambda = 8$ dB, the partial cooperation scheme can increase the mean sum rate by approximately 22% compared with the no-cooperation scheme. Assuming imperfect CCSI with a small error, $\varsigma = 0.99$, the partial cooperation scheme can still increase the mean sum rate by approximately 16% compared with the no-cooperation scheme.

Next we find the cooperation gain defined as (19) with respect to the threshold, Λ in Fig. 5. We assume the transmit SNR is 30 dB. $\Lambda = 0$ refers to no-cooperation.

The simulation results in Fig. 5 indicate that SLNR precoders perform almost the same as ZF precoders. If we set the threshold in the region $\Lambda > 50$ dB, the cooperation gain saturates as all users fall into the cooperation zone which is equivalent to the full cooperation scheme. The simulation results also demonstrate that imperfect CCSI significantly reduces the cooperation gain. For example, the full cooperation scheme encounters a very significant drop in cooperation gain with imperfect CCSI, from 3.48 to 2.94 and 2.19 for $\varsigma = 0.99$ and $\varsigma = 0.95$, respectively.

Table 2 Outage probability for urban users

Outage probability percentage, %		
	ZF precoders	SLNR precoders
full cooperation	13.60	13.25
partial cooperation	14.45	13.89
partial cooperation $\varsigma = 0.99$	16.11	15.33
no cooperation	28.26	27.71

In Table 2, we give the outage probabilities for urban users at 30 dB transmit SNR. It can be seen that, the SLNR precoders outperform the ZF precoders by a small margin as expected, which is consistent with the results in Fig. 4. We also note that the outage probability with partial cooperation is significantly higher than no cooperation scheme as partial-cooperation improves the gains for cell-edge users in particular. Majority of the users which are below the chosen threshold are also located in the cooperation zone. Therefore, the outage probabilities with partial cooperation scheme is close to the outage probabilities with full cooperation scheme.

4.2.2 Suburban area performance comparisons: Next, we evaluate the simulations for users in suburban areas. In Fig. 6, the mean sum rates (20) are given for suburban users.

The results in Fig. 6 demonstrate that SLNR precoders provide better sum rates than ZF precoders from very low transmit SNRs up to 35 dB, after which they provide approximately the same performace as ZF precoders. Here, we also observe that the performance of SLNR precoders approaches the performance of ZF precoders at higher transmit SNRs, compared with urban users. The reason is the fact that the interference levels are lower for suburban users as seen in Fig. 3. We also observe in Fig. 6 that partial cooperation with imperfect CCSI where $\varsigma = 0.99$ provides better mean sum rates compared with the no-cooperation scheme. For instance, at transmit SNR 40 dB, the partial cooperation scheme achieves approximately 5 bits/s/Hz of mean sum rates, while the mean sum rates for no cooperation scheme at same transmit SNR is approximately 4 bits/s/Hz.

In Fig. 7, we investigate the cooperation gain (19) vs threshold, Λ, for suburban users. We assume that the transmit SNR = 30 dB.

As seen in Fig. 7, the full cooperation scheme suffers a drop in cooperation gain with imperfect CCSI, from approximately 3.39 to 2.30 and 2.09 for $\varsigma = 0.99$ and $\varsigma = 0.95$, respectively. We note that the cooperation gains for suburban areas are lower than urban areas because interference for suburban areas is less than the interference in urban areas as shown in Figs. 2 and 3. However, suburban users suffer a loss in cooperation gain with imperfect

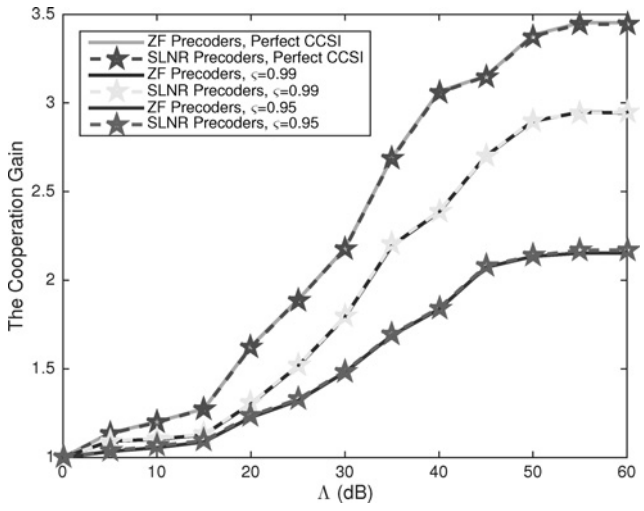

Fig. 5 *Cooperation gain for urban users*

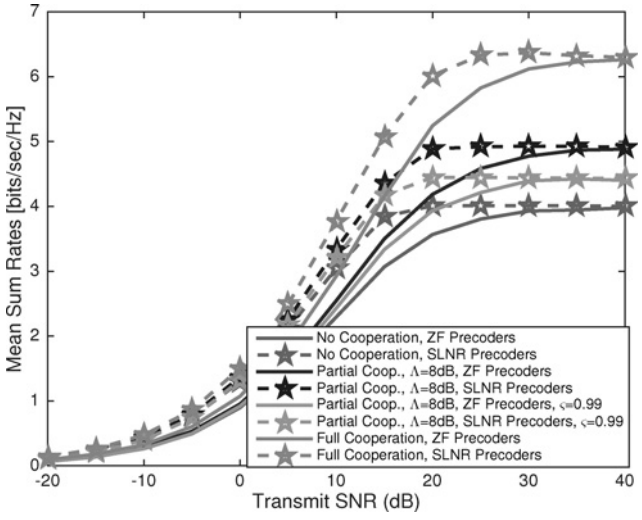

Fig. 6 *Mean sum rates for suburban users*

© The Institution of Engineering and Technology 2016

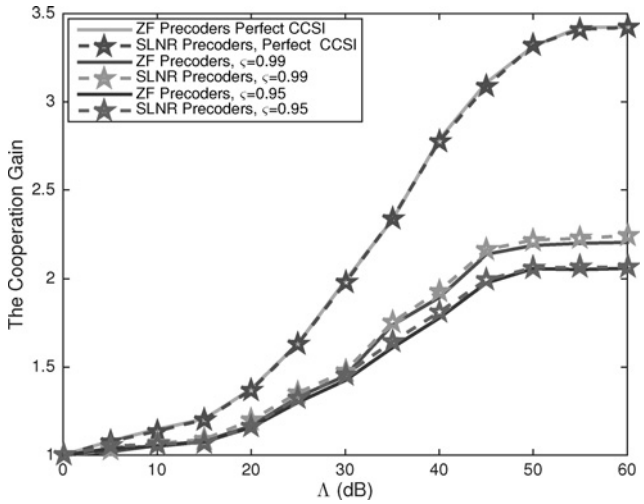

Fig. 7 *Cooperation gain for suburban users*

Table 3 Outage probability for suburban users

Outage probability percentage, %		
	ZF precoders	SLNR precoders
full cooperation	14.25	12.23
partial cooperation	15.75	13.10
partial cooperation $\varsigma = 0.99$	20.19	17.33
no coopeartion	29.81	27.10

CCSI more than urban area users, because the unknown remaining interference is also less for suburban areas as given in Section 4.1. The dominant interference, for which cross-channels are known and cancelled at the receiver, take up more of the total interference for suburban area users. In other words, the γ ratio is lower for suburban users. This explains why the imperfect CCSI impacts these users more than urban area users.

The outage probabilities for suburban users at transmit SNR 30 dB are given in Table 3. Once again, the SLNR precoders perform better than the ZF precoders, which is consistent with Fig. 6. The results also indicate that partial cooperation provides significant gain compared with no cooperation scheme. We also observe that imperfect CCSI increases the outage probabilities significantly, and this increase is higher for suburban users than urban users. For example, for suburban users the outage probability increases from 13.10 to 17.33% with SLNR precoders for suburban users with imperfect CCSI. However, for urban users employed with SLNR precoders, the imperfect CCSI increases the outage probability from 13.89 to 15.33%, as given in Table 2.

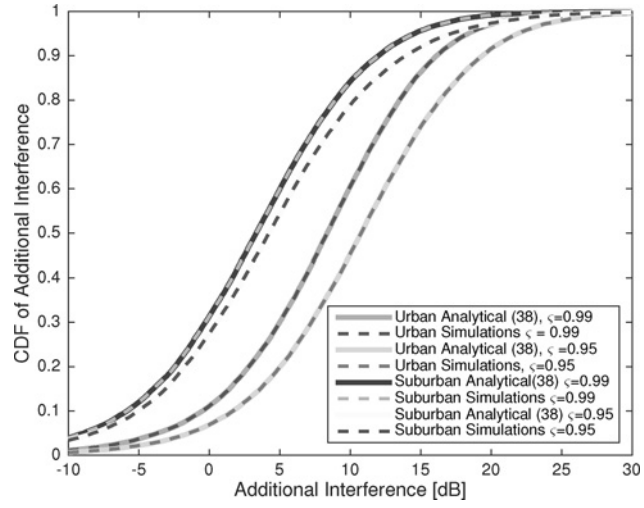

Fig. 8 *CDF of additional interference that is caused by imperfect CCSI*

4.2.3 Imperfect CCSI analysis: Finally, we investigate the accuracy of (38). We plot the CDF of additional interference that is caused by imperfect CCSI, assuming a transmit SNR at 30 dB and $\varsigma = 0.99, 0.95$ for urban and suburban users.

In Fig. 8, it is observed that (38) is matching with the simulation results. Therefore, we verify the accuracy of (38). As seen in this figure, the additional interference increases as ς decreases due to the reduced accuracy in the channel estimation. We also note that the additional interference for urban users is more than for suburban users as a result of path loss differences.

5 Conclusions

In this paper, we have investigated a partial cooperative interference cancellation scheme in a downlink cellular network. We have proposed that the cooperative users in the cooperation zone use MMSE receivers and can cancel intercell interference using CCSI from neighbouring cells. Other users located outside the cooperation zone have been assumed to use MF receivers. We have shown that the system achieves better sum rates with cooperation, provided there is reasonable CCSI accuracy. Setting the cooperation threshold as 8 dB, we have demonstrated that the partial cooperative scheme can achieve gains of approximately 25% in mean sum rates relative to the no-cooperation scheme at a transmit SNR of 40 dB. We have considered urban and suburban environments and computed the ratio of the users falling in the overlapping regions (i.e. subject to cooperation) for urban and suburban environments. We have also calculated the SNR, SINR levels for each of these environments. We have compared the results for ZF and SLNR-based precoders and shown that SLNR-based precoders achieve better sum rates at low transmit SNRs while their performance is equivalent to ZF precoders at high transmit SNRs. However, we have also shown that the transmit SNR value at which the performance of SLNR precoders approaches that of ZF precoders is different for different environments. For suburban users, this value is higher than for urban areas, because of lower interference levels. We have also considered imperfect CCSI between the cooperative users and interfering BSs. We have derived analytical expressions for the additional interference caused by imperfect CCSI. We have demonstrated that imperfect CCSI causes a degradation in system performance. We have also shown that the imperfect CCSI impacts the users in suburban areas more than the users in urban areas because the remaining interference levels are lower for these users than the users in urban areas. We have also provided an analytical expression for additional interference caused by imperfect CCSI. We have confirmed the accuracy of this analytical expression via simulation results which show that analytical expression perfectly matches with the simulation results. We have also noted that the additional interference for urban users is more than for suburban users as a result of path loss differences.

6 References

1 Cadambe, V., Jafar, S.: 'Interference alignment and the degrees of freedom of the K user interference channel', *IEEE Trans. Inf. Theory*, 2008, **54**, (8), pp. 3425–3441
2 Maham, B., Popovski, P.: 'Cognitive multiple-antenna network with outage and rate margins at the primary system', *IEEE Trans. Veh. Technol.*, 2015, **64**, (6), pp. 2409–2422
3 Gou, T., Jafar, S.: 'Degrees of freedom of the K user $M \times N$ MIMO interference channel', *IEEE Trans. Inf. Theory*, 2010, **56**, (8), pp. 6040–6057
4 El Ayach, O., Peters, S., Heath, J.R.: 'The practical challenges of interference alignment', *IEEE Wirel. Mag.*, 2013, **20**, (8), pp. 35–42
5 Suh, C., Ho, M., Tse, D.: 'Downlink interference alignment', *IEEE Trans. Commun.*, 2011, **59**, (9), pp. 2616–2626
6 Ustok, R.F., Shafi, M., Dmochowski, P.A., *et al.*: 'Interference alignment with combined receivers with heterogeneous networks'. Proc. of IEEE Conf. on Communications, Sydney, Australia, June 2014, pp. 35–40

© The Institution of Engineering and Technology 2016

7 Spencer, Q., Swindlehurst, A., Haardt, M.: 'Zero-forcing methods for downlink spatial multiplexing in multiuser MIMO channels', *IEEE Trans. Signal Process.*, 2004, **52**, (2), pp. 461–471
8 Sadek, M., Tarighat, A., Sayed, A.: 'A leakage-based precoding scheme for downlink multi-user MIMO channels', *IEEE Trans. Wirel. Commun.*, 2007, **6**, (5), pp. 1711–1721
9 Ai, T., Wu, Z.: 'Interference mitigation for downlink base station cooperation with joint distributed space-time coding'. Proc. of IET Wireless Mobile and Computing Conf., Shanghai, China, June 2011, pp. 201–206
10 Jang, U., Lee, K., Cho, K.S., *et al.*: 'Downlink transmit beamforming for intercell interference mitigation with BS cooperation'. Proc. of IEEE Global Telecommunications Conf., Miami, USA, December 2010, pp. 1–5
11 Caire, G., Ramprashad, H., Papadopolous, C., *et al.*: 'Multiuser MIMO downlink with limited inter-cell cooperation: approximate interference alignment in time, frequency and space'. Proc. Annual Allerton Conf. on Communications, Control and Computing, Monticello, USA, September 2008, pp. 730–737
12 3GPP: 'CoMP operation for LTE physical layer aspects Release 11' (3GPP TR 25.996 version 6.1.0, ETSI TR 36.918 V0.0.1, 2011)
13 Guedes, L.G., Yacoub, M.: 'Overlapping cell area in different fading conditions'. Proc. of IEEE Vehicular Technology Conf., Chicago, USA, July 1995, pp. 380–383
14 Wang, Z., Xiao, M., Wang, C., *et al.*: 'Degrees of freedom of two-hop MISO broadcast networks with mixed CSIT', *IEEE Trans. Wirel. Commun.*, 2014, **13**, (12), pp. 6982–6995
15 Ustok, R.F., Shafi, M., Dmochowski, P.A., *et al.*: 'Aligned interference neutralisation for $2 \times 2 \times 2$ interference channel with imperfect channel state information'. Proc. of IEEE Conf. on Communications, Budapest, Hungary, June 2013, pp. 5230–5235
16 Suraweera, H.A., Smith, P.J., Shafi, M.: 'Capacity limits and performance analysis of cognitive radio with imperfect channel knowledge', *IEEE Trans. Veh. Technol.*, 2010, **59**, (4), pp. 1811–1822
17 Wang, Z., Chen, W.: 'Regularized zero-forcing for multiantenna broadcast channels with user selection', *IEEE Wirel. Commun. Lett.*, 2012, **1**, (2), pp. 129–132
18 Yuan, F., Yang, C.: 'Equivalence of SLNR precoder and RZF precoder in downlink MU-MIMO systems', ArXiv e-prints, available at http://arxiv.org/abs/1202.1888, published in 2012
19 Sadek, M., Tarighat, A., Sayed, A.: 'Active antenna selection in multi user MIMO communications', *IEEE Trans. Signal Process.*, 2007, **55**, (4), pp. 1498–1510
20 Ahn, K., Heath, R.: 'Performance analysis of maximum ratio combining with imperfect channel estimation in the presence of cochannel interferences', *IEEE Trans. Wirel. Commun.*, 2009, **8**, (3), pp. 1080–1085
21 Marzetta, T.: 'BLAST training: Estimating channel characteristics for high capacity space-time wireless'. Proc. of Annual Allerton Conf. on Communications, Control and Computing, Monticello, USA, September 2009, pp. 958–966
22 Miller, S.K.: 'On the inverse of the sum of matrices', *Math. Mag.*, 1981, **54**, (3), pp. 67–72
23 3GPP: 'Universal Mobile Telecommunications System (UMTS); spatial channel model for Multiple Input Multiple Output (MIMO) simulations Release 10' (3GPP TR 25.996 version 6.1.0 Release 10., ETSI TR 125 996 V6.1.0, 2011)

© The Institution of Engineering and Technology 2016